

# Graphene as a sensor

Kazi Rafsanjani Amin\* and Aveek Bid

Department of Physics, Indian Institute of Science, Bangalore 560 012, India

**Graphene has emerged as one of the strongest candidates for post-silicon technologies. One of the most important applications of graphene in the foreseeable future is sensing of particles of gas molecules, biomolecules or different chemicals or sensing of radiation of particles like alpha, gamma or cosmic particles. Several unique properties of graphene such as its extremely small thickness, very low mass, large surface to volume ratio, very high absorption coefficient, high mobility of charge carriers, high mechanical strength and high Young's modulus make it exceptionally suitable for making sensors. In this article we review the state-of-the-art in the application of graphene as a material and radiation detector, focusing on the current experimental status, challenges and the excitement ahead.**

**Keywords:** Graphene, sensor, radiation detector, response and recovery time.

THE demonstration of the existence of a perfectly two-dimensional crystal, graphene was one of the most celebrated inventions in present-day condensed matter science<sup>1</sup>. Since then, graphene has been a focus of research, both from basic science as well as applied science. Most of the interesting features of electrical transport characteristics in graphene come from the linear dispersion of Dirac electrons. In pristine graphene, the conductance is expected to be a minimum, due to the Fermi energy lying at the charge neutrality point (Dirac point). By applying an electric field, which is usually done by the application of a gate voltage in graphene field-effect transistors, the entire band structure of graphene can be shifted with respect to the Fermi level. The density of states close to Fermi energy increases linearly with energy. Thus, by application of gate voltage, either electrons or holes can be induced in graphene channels which, in turn, give increasing conductivity with increasing magnitude of gate voltage on either side of the Dirac point<sup>2-4</sup>. Graphene layers are usually mechanically exfoliated from graphite<sup>1,5,6</sup> or are chemically grown using techniques like chemical vapour deposition<sup>7-15</sup>. The field-effect transistor fabrication usually involves electron beam lithographic process using polymer coating, exposure, metal deposition and lift-off. The devices fabricated in this way are usually left with residues of polymer or water, which cause signifi-

cant shift in charge neutrality point. The properties of these devices are observed to change upon exposure to ambient environment due to impurity deposition on graphene. This forms the motivation of applying monolayer graphene as sensors detecting particles or molecules.

Several unique properties of graphene make it exceptionally suitable for making sensors. Being a pure two-dimensional system, graphene represents the ultimate NEMS system with all its atoms exposed to the surface. In fact, the specific surface area (2630 m<sup>2</sup>/g) of graphene is amongst the highest in layered materials<sup>16</sup>. This makes the conductance of graphene extremely sensitive to the ambient and the presence of a single adsorbed molecule on its surface can significantly modify its electrical characteristics. Second, it is highly conductive even in very low carrier density regimes with room temperature mobilities of the order of 10,000 cm<sup>2</sup>/Vs routinely achievable<sup>17-19</sup>. Coupled with the high carrier concentration (10<sup>12</sup> cm<sup>-2</sup>), this makes the conductance of graphene monolayers larger than any metal at room temperature. This ensures that graphene-based sensors have extremely low levels of Johnson–Nyquist thermal noise compared to semiconductor-based sensors.

It also has fewer kinds of defects due to the high quality of its two-dimensional crystal structure<sup>1,20-22</sup> and hence has intrinsically low levels of 1/f noise arising out of thermal switching of defects<sup>23</sup>. Third, it is relatively easy to make four terminal measurements on graphene strips making contact resistances much easier to deal with than, for example, in carbon nanotubes, which share almost all other advantages of graphene. All these factors combine to give a very large signal-to-noise ratio in graphene sensors even at room temperatures, providing it the ability to detect changes in local charge concentration of less than the charge of a single electron. Fourth, graphene can interact with materials through a variety of interactions, from weak van der Waals force to extremely stable covalent bonds. This allows for detection of a wide variety of materials using graphene with very high specificity.

At low temperatures, where most of the mobile defects freeze out, the material and radiation sensitivity of graphene is unprecedented. It is predicted that at low temperatures, the charge sensing abilities of high-mobility graphene monolayers will rival those of radio-frequency single-electron transistors. On the mechanical side, suspended graphene flakes have been shown to have a very high Young's modulus (~ 1 TPa)<sup>24,25</sup> and to have a much

\*For correspondence. (e-mail: kazi@physics.iisc.ernet.in)

higher elasticity than membrane materials like silicon nitride commonly used in NEMS. Thus, despite thickness of just one monolayer, graphene maintains a high crystal-line order and can form the basis of NEMS of extremely small thickness, very low mass, large surface to volume ratio and high Young's modulus. Properties like atomically thin layers, very high absorption coefficient, high mobility of charge carriers and high mechanical strength make it an ideal candidate for use as radiation sensors. Making an effective sensor requires interface accessibility, good transduction, mechanical/electrical robustness, ease of preparation and integration into existing technologies. Graphene seems to satisfy this entire list of criteria and hence has the potential to emerge as the sensor material of choice in the future.

In addition to graphene, reduced graphene oxide (RGO) has also been tested as a sensor material<sup>26–31</sup> and found to be quite effective as a gas sensor. RGO, which can be bulk synthesized using relatively cheap chemical routes, can be made into ultra thin sensing layers by a variety of wet techniques such as casting, ink-jet printing<sup>32,33</sup>, Langmuir–Blodgett technique<sup>34,35</sup> and layer-by-layer deposition<sup>36</sup>. A big advantage of RGO over graphene is the relative ease with which it can be functionalized by other materials (like metal nanoparticles) to increase the specificity of detection.

In this article, we review the physics and applications of pristine graphene and RGO as gas and radiation sensors. In addition to pristine graphene and chemically modified graphene (e.g. RGO), composites of graphene with metal, metal oxides and polymers have also shown good promise as sensor materials<sup>29,30,37–46</sup>, these are, however, outside the scope of the present review.

## Graphene as a detector

The detection of gases by graphene materials is based on the changes in its electrical conductance due to the adsorption of gas molecules on its surface. These molecules act as donors or acceptors and hence change either the number density or the mobility of the carriers in graphene leading to a change in conductance. The interaction of the adsorbate with graphene depends on its electrical and chemical nature. Molecules having a closed shell structure modify the conductance of graphene by changing the local electronic distribution. Aromatic molecules, on the other hand, modify the transmission coefficients of the charge carriers and hence modify the conductance of the device<sup>47</sup>, and OH radicals can form covalent bonds with graphene and effect the hopping of electrons along the free bond.

The first successful application of graphene as a gas molecule sensor was reported by Schedin *et al.*<sup>48</sup> in 2007. The graphene field-effect transistor sensor devices were fabricated by mechanical cleavage of graphite on the

surface of highly doped silicon wafer having a 300 nm oxide layer, followed by conventional electron beam lithography process. The device was patterned in a hall bar geometry to allow simultaneous measurement of longitudinal ( $\rho_{xx}$ ) and transverse ( $\rho_{xy}$ ) resistivity. Measurement of  $\rho_{xy}$  in the magnetic field allowed one to calculate the change in charge carrier concentration directly. Gases like  $\text{NO}_2$ ,  $\text{NH}_3$ ,  $\text{H}_2\text{O}$  and  $\text{CO}$  were diluted till concentration of 1 ppm in pure helium or nitrogen gas in atmospheric pressure, and the graphene sensor devices were exposed to them. Measurement of change in  $\rho_{xx}$  with time upon exposure of gas molecules revealed the sensor action of the devices. Instant change in  $\rho_{xx}$  was observed as soon as gas molecules sat on graphene, and after a short time,  $\rho_{xx}$  saturated (Figure 1). The degassing process, although, does not occur readily. It was required to heat up the device to high temperatures ( $\approx 150^\circ\text{C}$ ) in high vacuum environment.

The nature of charge carrier doping depends on species, which is revealed from measurement of  $\rho_{xy}$ . If the sensing is started at either the hole-doped region or in the electron-doped region of graphene conduction, increase or decrease in resistivity will be observed depending upon the nature of charge carrier induced by the molecule sitting on it. The nature of charge carrier doping is presented in Table 1.

Subsequently, graphene has been successfully applied to sense carbon dioxide, hydrogen, oxygen and other gases. In 2010, Wu *et al.*<sup>49</sup> used graphene grown by chemical vapour deposition to sense hydrogen gas in air

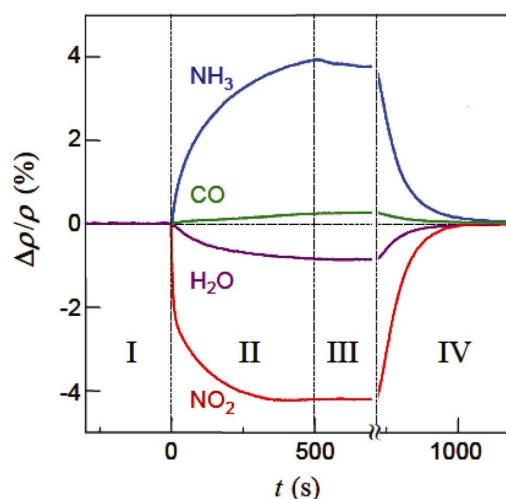


**Figure 1.** Change in resistivity due to exposure of graphene device to different gases (for details see text). Positive (negative) sign of change indicates electron (hole) doping in graphene. Section I: Graphene device kept in vacuum before exposure. Section II: Graphene device exposed to different gas molecules. A sharp change is observed as soon as the device is exposed. Section III: Resistivity reaches a steady value and does not change much on evacuation of the measurement system. Section IV: Degassing occurs on heating the graphene device to  $150^\circ\text{C}$  and resistance comes to starting value, indicating that the device has reached the pristine state (from ref. 48).

with concentration in the range 0.0025–1% (Figure 2). A 1 nm thin layer of palladium was deposited on the graphene by electron beam evaporation to enhance the H<sub>2</sub> sensing activity. The sensitivity of the sensor is defined

**Table 1.** Nature of charge carrier doping in graphene by different common chemicals

Species	Doping
Ethanol	Electron
CO	Electron
NH <sub>3</sub>	Electron
NO <sub>2</sub>	Hole
H <sub>2</sub> O	Hole
O <sub>2</sub>	Hole

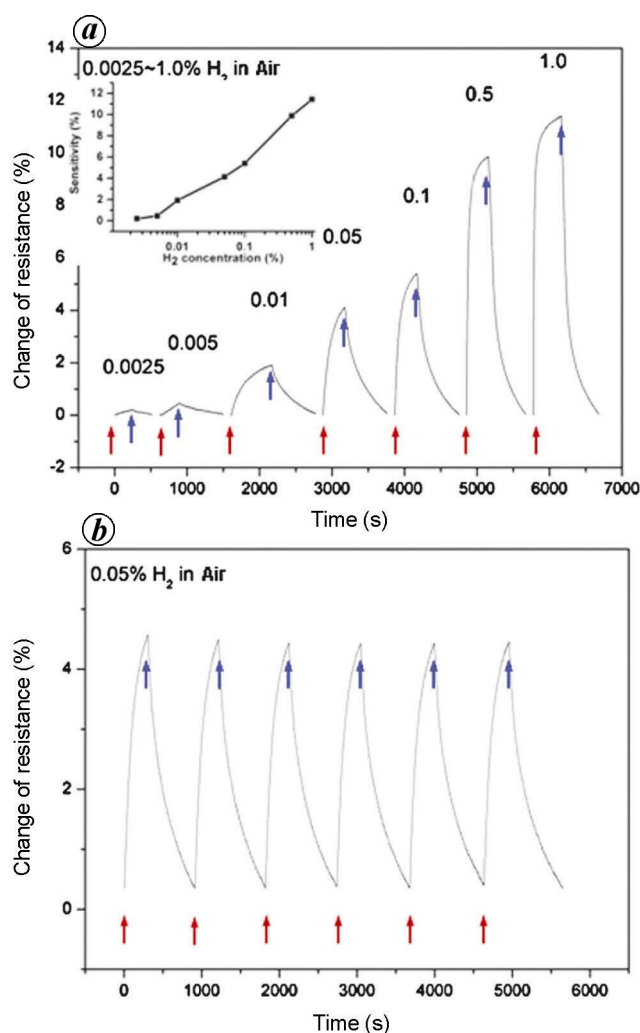


**Figure 2.** *a*, Change in resistance of graphene device from the pristine state is observed when the device is exposed to hydrogen gas at different concentrations (percentage of volume in dry air). The turn on event of gas is shown by red arrow, while blue arrow indicates beginning of flow of dry air. (Inset) Sensitivity of the device as a function of H<sub>2</sub> concentration in log scale. *b*, Reproducible response is observed when the sensor is exposed to a fixed concentration (0.05%) of H<sub>2</sub> six times (from ref. 49).

as  $(R_{\text{peak}} - R_0)/R_0 \times 100\%$ , where  $R_{\text{peak}}$  is the highest resistance of the sensor upon exposure to hydrogen gas, and  $R_0$  is resistance in ambient atmosphere. The sensitivity was found to increase as the hydrogen concentration in air increased. The behaviour is shown in Figure 2 inset, where the sensitivity is plotted with the logarithm of hydrogen concentration, and a linear nature is observed. The sensors show an increase of almost 10% in resistivity to exposure of 1% of hydrogen concentration. A measurable change in resistivity (0.2%) was also observed corresponding to an exposure of 25 ppm hydrogen concentration. The presence of palladium is important for the sensing action, as reported in similar works involving hydrogen detection also<sup>44,45</sup>. The electron beam evaporation leaves discrete palladium nanoparticles on graphene. On exposure to hydrogen, these get converted into PdH<sub>x</sub>, which is dipolar, with the hydrogen site being positive. Now if we see the molecular structure of the assembly, Pd sits directly on graphene, and the hydrogen part of the formed dipolar PdH<sub>x</sub> sits on the top surface. Thus, upon exposure to hydrogen gas, electrons accumulate in the interface between Pd and graphene carbon. The induced electrons cause change in resistivity of graphene. As the amount of hydrogen is increased, more electrons are induced in the graphene channel, leading to enhanced change in resistance. This is realized as increase in sensor sensitivity. Without palladium, the sensors do not show any appreciable change in resistivity, owing to the fact that direct interaction of hydrogen and carbon is very limited. Oxygen present in the air accelerates the degassing, and Pd acts as catalyst.

Graphene FET solid-state sensors were used by Yoon *et al.*<sup>50</sup> in 2011 to sense CO<sub>2</sub>. The graphene flakes were exfoliated from HOPG and transferred on oxidized silicon wafer with the aid of sticky polydimethylsiloxane (PDMS) stamps. The desired amount of carbon dioxide gas was mixed with highly purified nitrogen (79%) and oxygen gas (21%) and the graphene sensor device was exposed to it. CO<sub>2</sub> was found to get adsorbed on the graphene surface much faster than other gases, because the response time (time taken by the sensor to reach steady state after exposure to gas) was much smaller. The sensitivity of the sensor was linear, 0.17% per ppm of CO<sub>2</sub> in air with concentration in the range 10–100 ppm (Figure 3). Chen *et al.*<sup>51</sup> showed reproducible oxygen gas sensitivity using wafer-scale CVD-grown graphene, transferred on oxidized silicon wafer. Oxygen gas molecules attached on the surface of graphene enhance hole transport, which in turn, causes change in resistivity.

Graphene-based sensors not only show high sensitivity with good reproducibility, they also allow detection of very small amount of subject gas molecule. Chen *et al.*<sup>53</sup> showed detection of sub ppt concentration of different gas molecules like NH<sub>3</sub>, NO, NO<sub>2</sub>, N<sub>2</sub>O, etc. Ozone-treated graphene allowed enhancement in performance of the detection of NO<sub>2</sub> gas with extremely low, down to

parts per billion concentration<sup>42</sup>. In another study, graphene sensor was exposed to strongly diluted NO<sub>2</sub> gas. The change in transverse resistivity ( $\rho_{xy}$ ) was observed to occur not continuously, but in discrete steps. Similar steps in  $\rho_{xy}$  were also observed during the gas desorption process<sup>48</sup>. These steps were attributed to addition/subtraction of single electron from graphene channel (Figure 4).

Although there have been many reports showing sensing application of graphene with good reproducibility, detecting the type of gas molecule sitting on graphene with confirmation was difficult. Rumyantsev *et al.*<sup>53</sup> reported a

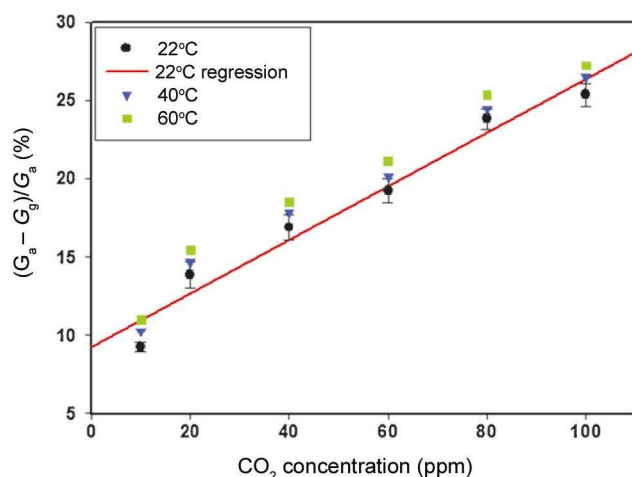


**Figure 3.** Change in conductance of graphene sensor device as a function of CO<sub>2</sub> concentration. Similar result is observed when the device is operated at the three mentioned temperatures (from ref. 50).

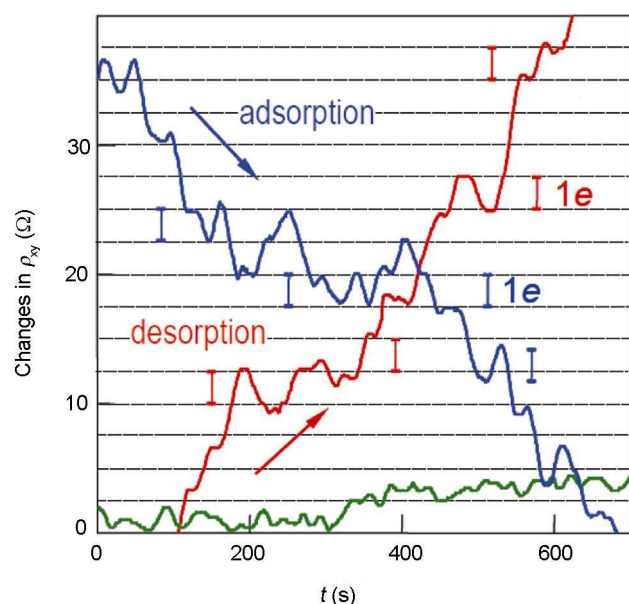


**Figure 4.** The Hall resistance jumps during gas molecule absorption and desorption on graphene. The green line is response obtained when the device, after annealing, is kept in pure helium environment. Jumps caused by single-electron addition (or subtraction) correspond to the grid lines (from ref. 48).

method based on low frequency conductance fluctuation. Graphene field-effect devices, fabricated by mechanical exfoliation followed by standard electron beam lithography, were exposed to vapours of different gases and low frequency  $1/f$  noise (conductance fluctuation) was measured using a spectrum analyser. Characteristic bulges over the  $1/f$  power spectrum were observed, where the characteristic frequency is different for different types of gas molecules (Figure 5). The appearance of the characteristic frequency in  $1/f$  noise spectrum can be attributed to kinetics of adsorption–desorption mechanism of different types of gas molecules, which has different timescales for different species. Again, different gas molecules can give rise to specific traps and scattering centres, which give rise to conducting fluctuation with certain timescale, which, in turn, may give rise to these characteristic frequencies.

Graphene has not only been applied successfully for detecting chemical vapours of different types; a lot of effort is on going to apply graphene transistor as a radiation sensor<sup>54–56</sup>. Foxe *et al.*<sup>55</sup> applied graphene transistor, fabricated on SiC substrate, to detect alpha particle radiation. A 3.4  $\mu\text{m}$  <sup>10</sup>B conversion layer was chosen based on Monte Carlo simulations to generate detectable  $\alpha$ -particle signal. Neutron hitting the layer of <sup>10</sup>B of the specified layer gives rise to  $\alpha$ -particle with 1.78 MeV energy. A measurable change in slope of transfer characteristics ( $RV_G$  curve) was observed after the device was exposed to radiation. The observations are summarized in Table 2.

Electron beam radiation causes a shift in Dirac point of graphene and changes the mobility of graphene. Graphene, fabricated by electron beam lithography, usually

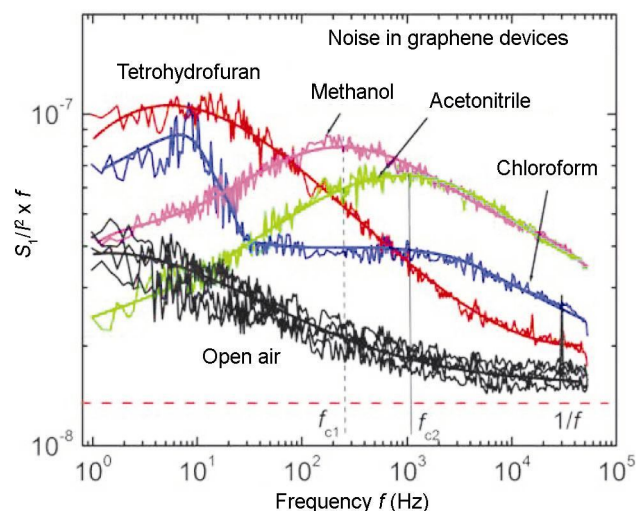


**Figure 5.** The  $1/f$  noise power spectrum of graphene device under exposure to different gas vapours (shown in different colours). The power spectral density is scaled by  $fI^2$  to make the spectrum independent of frequency and current passing in the device. Different vapours introduce noise with specific characteristic frequency, which shows up as a bulge over the expected flat scaled noise spectrum (from ref. 53).

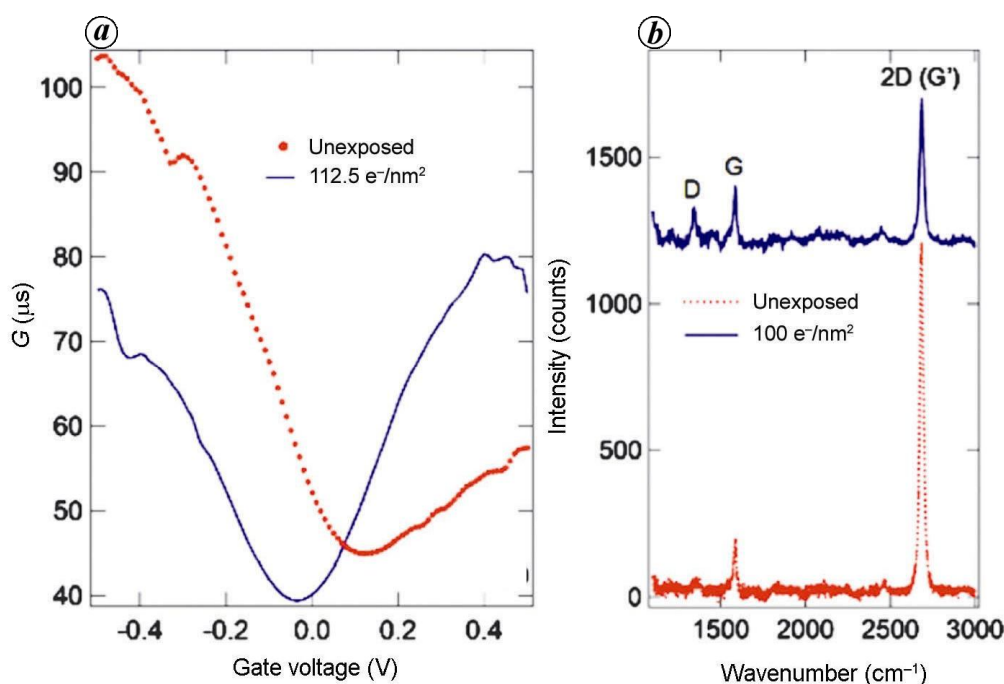


**Figure 6.** Effect of electron beam irradiation is summarized in brief. *a*, Dirac point is observed to shift to the more negative gate voltage upon exposure of a device with electron beam, with mentioned dosage. *b*, Disorder induced *D* peak shows up in Raman spectra after a similar device is exposed to electron beam, indicating formation of defect in graphene sheet caused by the electron beam. The spectra have been shifted for clarity (from ref. 56).

**Table 2.** Change in slope of  $RI_V$  curve caused by  $\alpha$ -particle radiation<sup>55</sup>

Event	Slope ( $\text{k}\Omega/\text{V}$ )
No. post	$-135 \pm 10$
$\alpha$ post	$-54 \pm 3$

becomes hole-doped at the end of the process, which is related to residues of polymer and water molecules of the environment left on graphene. Thus, low dosage of electron beam neutralizes the additional hole doped and shifts the experimental Dirac point towards 0 V. As reported by Childres *et al.*<sup>56</sup>, for a typical graphene FET, the experimental Dirac point was found to shift to 4.9 V from 16.3 V after the device was exposed to a electron dose of  $112.5 e^-/\text{nm}^2$ . After the device was exposed multiple times, accumulating a total dose of  $4500 e^-/\text{nm}^2$ , the Dirac point shifted to  $-3.8$  V and the mobility was reduced by 5 to 6 times (Figure 6). The electron beam irradiation generated electron-hole pairs, and the holes, being less mobile, get trapped in the graphene-SiO<sub>2</sub> interface. This generated electron-hole pairs induce electric field at the interface between SiO<sub>2</sub> and graphene, which adds to the electric field applied by back gate. Similar experiment on suspended graphene, where the oxide underneath the graphene was chemically etched, shows lesser shift in Dirac point, indicating the importance of

the presence of SiO<sub>2</sub> substrate. Raman spectroscopy revealed disorder-induced *D* peaks, revealing defects in lattice structure caused by electron beam on graphene layer<sup>57,58</sup> (Figure 6). This observation reveals that microscopy of graphene like SEM, TEM causes additional defects in it, which limit its mobility.

## Conclusions

In terms of sensitivity and selectivity graphene-based sensors are comparable to, and sometimes more effective than the state-of-the-art solid-state sensors. They have attractive features like room-temperature applications, very low energy activation arising from zero band gap, low fabrication cost, etc. However, there exist certain limiting factors which inhibit its widespread commercial application. Room-temperature hysteresis, which is common in graphene devices, make the response of the devices uncertain. Although the response time of the devices is fast, the recovery time of these devices is slow; it can take a graphene device up to thousands of seconds to reach back to its pristine condition. Presence of impurities on the surface from fabrication process causes the devices to be different from each other, which makes extracting a universal behaviour difficult. Some theoretical predictions and experimental results show that the presence of foreign chemicals or defects improves the sensor

action<sup>59–61</sup>. The highest quality graphene is still obtained by exfoliation of graphite – a process not amenable to industrial-scale production. New graphene production techniques, device fabrication methods and experiments must be designed addressing these problems if graphene devices are to emerge as the next-generation smart sensors.

- Novoselov, K. S. *et al.*, Electric field effect in atomically thin carbon films. *Science*, 2004, **306**, 666–669.
- Castro Neto, A. H., Guinea, F., Peres, N. M. R., Novoselov, K. S. and Geim, A. K., The electronic properties of graphene. *Rev. Mod. Phys.*, 2009, **81**, 109–162.
- Das Sarma, S., Adam, S., Hwang, E. H. and Rossi, E., Electronic transport in two-dimensional graphene. *Rev. Mod. Phys.*, 2011, **83**, 407–470.
- Peres, N. M. R., The transport properties of graphene. *J. Phys.: Condens. Matter*, 2009, **21**, 323201.
- Novoselov, K. S. *et al.*, Two-dimensional gas of massless dirac fermions in graphene. *Nature*, 2005, 197200.
- Geim, A. K., Graphene: status and prospects. *Science*, 2009, **324**, 1530–1534.
- Li, X. *et al.*, Large-area synthesis of high-quality and uniform graphene films on copper foils. *Science*, 2009, **324**, 1312–1314.
- Yu, Q., Lian, J., Siriponglert, S., Li, H., Chen, Y. P. and Pei, S.-S., Graphene segregated on Ni surfaces and transferred to insulators. *Appl. Phys. Lett.*, 2008, **93**, 113103.
- Li, X., Wang, X., Zhang, L., Lee, S. and Dai, H., Chemically derived, ultrasmooth graphene nanoribbon semiconductors. *Science*, 2008, **319**, 1229–1232.
- Bae, S. *et al.*, Roll-to-roll production of 30-inch graphene films for transparent electrodes. *Nat. Nanotechnol.*, 2010, **5**, 574–578.
- Yan, K., Peng, H., Zhou, Y., Li, H. and Liu, Z., Formation of bilayer bernal graphene: layer-by-layer epitaxy via chemical vapor deposition. *Nano Lett.*, 2011, **11**, 1106–1110.
- Li, X. *et al.*, Graphene films with large domain size by a two-step chemical vapor deposition process. *Nano Lett.*, 2010, **10**, 4328–4334.
- Mattevi, C., Kim, H. and Chhowalla, M., A review of chemical vapour deposition of graphene on copper. *J. Mater. Chem.*, 2011, **21**, 3324–3334.
- Losurdo, M., Giangregorio, M. M., Capezzuto, P. and Bruno, G., Graphene cvd growth on copper and nickel: role of hydrogen in kinetics and structure. *Phys. Chem. Chem. Phys.*, 2011, **13**, 20836–20843.
- Reina, A. *et al.*, Large area, few-layer graphene films on arbitrary substrates by chemical vapor deposition. *Nano Lett.*, 2009, **9**, 30–35.
- Pumera, M., Ambrosi, A., Bonanni, A., Chng, E. L. K. and Poh, H. L., Graphene for electrochemical sensing and biosensing. *TrAC Trends Anal. Chem.*, 2010, **29**, 954–965.
- Soldano, C., Mahmood, A. and Dujardin, E., Production, properties and potential of graphene. *Carbon*, 2010, **48**, 2127–2150.
- Zheng, M. *et al.*, Metal-catalysed crystallization of amorphous carbon to graphene. *Appl. Phys. Lett.*, 2010, **96**, 063110.
- Abergel, D. S. L., Apalkov, V., Berashevich, J., Ziegler, K. and Chakraborty, T., Properties of graphene: a theoretical perspective. *Adv. Phys.*, 2010, **59**, 261–482; arXiv:1003.0391[cond-mat.mtrl-sci].
- Lin, Y.-M. and Avouris, P., Strong suppression of electrical noise in bilayer graphene nanodevices. *Nano Lett.*, 2008, **8**, 2119–2125.
- Ratinac, K. R., Yang, W., Ringer, S. P. and Braet, F., Toward ubiquitous environmental gas sensors capitalizing on the promise of graphene. *Environ. Sci. Technol.*, 2010, **44**, 1167–1176.
- Shao, Q., Liu, G., Teweldebrhan, D., Balandin, A. A., Rumyantsev, S., Shur, M. S. and Yan, D., Flicker noise in bilayer graphene transistors. *IEEE Electron Device Lett.*, 2009, **30**, 288–290.
- Dutta, P. and Horn, P. M., Low-frequency fluctuations in solids:  $1/f$  noise. *Rev. Mod. Phys.*, 1981, **53**, 497–516.
- Frank, I. W., Tanenbaum, D. M., van der Zande, A. M. and McEuen, P. L., Mechanical properties of suspended graphene sheets. *J. Vac. Sci. Technol. B*, 2007, **25**, 2558.
- Lau, C. N., Bao, W. and Jairo Velasco Jr, Properties of suspended graphene membranes. *Mater. Today*, 2012, **15**, 238–245.
- Li, W. *et al.*, Reduced graphene oxide electrically contacted graphene sensor for highly sensitive nitric oxide detection. *ACS Nano*, 2011, **5**, 6955–6961.
- Lu, G., Ocola, L. E. and Chen, J., Reduced graphene oxide for room-temperature gas sensors. *Nanotechnology*, 2009, **20**, 445502.
- Robinson, J. T., Keith Perkins, F., Snow, E. S., Wei, Z. and Sheehan, P. E., Reduced graphene oxide molecular sensors. *Nano Lett.*, 2008, **8**, 3137–3140.
- Mao, S., Cui, S., Lu, G., Yu, K., Wen, Z. and Chen, J., Tuning gas-sensing properties of reduced graphene oxide using tin oxide nanocrystals. *J. Mater. Chem.*, 2012, **22**, 11009–11013.
- Deng, S. *et al.*, Reduced graphene oxide conjugated Cu<sub>2</sub>O nanowire mesocrystals for high-performance NO<sub>2</sub> gas sensor. *J. Am. Chem. Soc.*, 2012, **134**, 4905–4917.
- Lu, G., Ocola, L. E. and Chen, J., Gas detection using low-temperature reduced graphene oxide sheets. *Appl. Phys. Lett.*, 2009, **94**, 083111–083111-3.
- Dua, V. *et al.*, All-organic vapor sensor using inkjet-printed reduced graphene oxide. *Angew. Chem. Int. Edn. Engl.*, 2010, **49**, 2154–2157.
- Le, L. T., Ervin, M. H., Qiu, H., Fuchs, B. E. and Lee, W. Y., Graphene supercapacitor electrodes fabricated by inkjet printing and thermal reduction of graphene oxide. *Electrochem. Commun.*, 2011, **13**, 355–358.
- Cote, L. J., Kim, F. and Huang, J., Langmuir–Blodgett assembly of graphene oxide single layers. *J. Am. Chem. Soc.*, 2009, **131**, 1043–1049.
- Li, X., Zhang, X., Bai, G., Sun, X., Wang, X., Wang, E. and Dai, H., Highly conducting graphene sheets and Langmuir–Blodgett films. *Nature Nanotechnol.*, 2008, **3**, 538–542.
- Dimiev, A., Kosynkin, D. V., Sinitskii, A., Slesarev, A., Sun, Z. and Tour, J. M., Layer-by-layer removal of graphene for device patterning. *Science*, 2011, **331**, 1168–1172.
- Kaniyoor, A., Imran Jafri, R., Arockiadoss, T. and Ramaprabhu, S., Nanostructured Pt decorated graphene and multi walled carbon nanotube based room temperature hydrogen gas sensor. *Nano-scale*, 2009, **1**, 382–386.
- Kang, X., Wang, J., Wu, H., Liu, J., Aksay, I. A. and Lin, Y., A graphene-based electrochemical sensor for sensitive detection of paracetamol. *Talanta*, 2010, **81**, 754–759.
- Guo, C. X., Lei, Y. and Li, C. M., Porphyrin functionalized graphene for sensitive electrochemical detection of ultratrace explosives. *Electroanalysis*, 2011, **23**, 885–893.
- Ang, P. K., Chen, W., Wee, A. T. S. and Loh, K. P., Solution-gated epitaxial graphene as Ph sensor. *J. Am. Chem. Soc.*, 2008, **130**, 14392–14393.
- Lu, Y., Goldsmith, B. R., Kybert, N. J. and Johnson, A. T. C., DNA-decorated graphene chemical sensors. *Appl. Phys. Lett.*, 2010, **97**, 083107–083107-3.
- Chung, M. G. *et al.*, Highly sensitive {NO<sub>2</sub>} gas sensor based on ozone treated graphene. *Sensors Actuators B: Chem.*, 2012, **166–167**, 172–176.
- Al-Mashat, L. *et al.*, Graphene/polyaniline nanocomposite for hydrogen sensing. *J. Phys. Chem. C*, 2010, **114**, 16168–16173.
- Lange, U., Hirsch, T., Mirsky, V. M. and Wolfbeis, O. S., Hydrogen sensor based on a graphene palladium nanocomposite. *Electrochim. Acta*, 2011, **56**, 3707–3712.

45. Chung, M. G. *et al.*, Flexible hydrogen sensors using graphene with palladium nanoparticle decoration. *Sensors Actuators B: Chem.*, 2012, **169**, 387–392.
46. Cuong, T. V. *et al.*, Solution-processed ZnO-chemically converted graphene gas sensor. *Mater. Lett.*, 2010, **64**, 2479–2482.
47. Chowdhury, R., Adhikari, S., Rees, P., Wilks, S. P. and Scarpa, F., Graphene-based biosensor using transport properties. *Phys. Rev. B*, 2011, **83**, 045401.
48. Schedin, F., Geim, A. K., Morozov, S. V., Hill, E. W., Blake, P., Katsnelson, M. I. and Novoselov, K. S., Detection of individual gas molecules adsorbed on graphene. *Nat. Mater.*, 2007, **6**, 652–655.
49. Wu, W. *et al.*, Wafer-scale synthesis of graphene by chemical vapor deposition and its application in hydrogen sensing. *Sensors Actuators B*, 2010, **150**, 296–300.
50. Yoon, H. J., Jun, D. H., Yang, J. H., Zhou, Z., Yang, S. S. and Cheng, M. M.-C., Carbon dioxide gas sensor using a graphene sheet. *Sensors Actuators B: Chem.*, 2011, **157**, 310–313.
51. Chen, C. W. *et al.*, Oxygen sensors made by monolayer graphene under room temperature. *Appl. Phys. Lett.*, 2011, **99**, 243502.
52. Chen, G., Paronyan, T. M. and Harutyunyan, A. R., Sub-ppt gas detection with pristine graphene. *Appl. Phys. Lett.*, 2012, **101**, 053119.
53. Rumyantsev, S., Liu, G., Shur, M. S., Potyralo, R. A. and Balandin, A. A., Selective gas sensing with a single pristine graphene transistor. *Nano Lett.*, 2012, **12**, 2294–2298.
54. Patil, A. *et al.*, Graphene field effect transistor as radiation sensor. In Nuclear Science Symposium and Medical Imaging Conference (NSS/MIC), IEEE, Valencia Convention Center, Valencia, Spain, 2011, pp. 455–459.
55. Foxe, M. *et al.*, Graphene-based neutron detectors. In Nuclear Science Symposium and Medical Imaging Conference (NSS/MIC), IEEE, Valencia Convention Center, Valencia, Spain, 2011, pp. 352–355.
56. Childres, I., Jauregui, L. A., Foxe, M., Tian, J., Jalilian, R., Jovanovic, I. and Chen, Y. P., Effect of electron-beam irradiation on graphene field effect devices. *Appl. Phys. Lett.*, 2010, **97**, 173109.
57. Ferrari, A. C. *et al.*, Raman spectrum of graphene and graphene layers. *Phys. Rev. Lett.*, 2006, **97**, 187401.
58. Ferrari, A. C., Raman spectroscopy of graphene and graphite: Disorder, electron-phonon coupling, doping and nonadiabatic effects. *Solid State Commun.*, 2007, **143**, 47–57.
59. Zhang, Y.-H., Chen, Y.-B., Zhou, K.-G., Liu, C.-H., Zeng, J., Zhang, H.-L. and Peng, Y., Improving gas sensing properties of graphene by introducing dopants and defects: a first-principles study. *Nanotechnology*, 2009, **20**, 185504.
60. Dan, Y., Lu, Y., Kybert, N. J., Luo, Z. and Johnson, A. T. C., Intrinsic response of graphene vapor sensors. *Nano Lett.*, 2009, **9**, 1472–1475.
61. Dai, J., Yuan, J. and Giannozzi, P., Gas adsorption on graphene doped with b, n, al, and s: A theoretical study. *Appl. Phys. Lett.*, 2009, **95**, 232105–232105-3.

ACKNOWLEDGEMENTS. This work was partially supported by the National Program on Micro and Smart Systems (NPMAS), Government of India. K.R.A. thanks CSIR, New Delhi for a fellowship.